AMERICAN Journal of Engineering, Mechanics and Architecture

Volume 4, Issue 08, 2026 ISSN (E): 2993-2637

Stress Assessment of Filleted Stepped Shafts under Combined Bending and Torsion

Mudher Naeem Yasir

Department of Materials Engineering, College of Engineering

Abstract: *Stepped shafts require diameter transitions for bearings, gears, couplings, and other mounted components, but the resulting shoulder fillet may govern the local stress. This study presents a dimensionless assessment of circular filleted shafts under combined bending and torsion. A finite-element-based correlation for the von Mises stress-concentration factor was applied to 60 combinations of diameter ratio D/d, fillet-radius ratio r/d, and nominal torsion-to-bending stress ratio η, covering $D/d = 1.2–1.8$, $r/d = 0.02–0.10$, and $\eta = 0–1$. For a 30 mm steel shaft with a nominal bending stress of 70 MPa and a yield strength of 355 MPa, the calculated stress-concentration factor ranged from 1.440 to 2.934. Increasing r/d from 0.02 to 0.10 reduced the factor by 32.8–42.5%, whereas increasing D/d from 1.2 to 1.8 raised it by 5.5–15.2%. Although the normalized factor decreased with increasing torsional contribution, the maximum local equivalent stress increased because of the higher nominal multiaxial stress. Under equal nominal bending and torsional stresses, the most severe case reached 343.4 MPa with a static safety factor of 1.03. For a required safety factor of 1.5, the minimum r/d increased from 0.0479 to 0.0653 as D/d increased from 1.2 to 1.8. Benchmark and representative finite-element comparisons showed deviations below 2.1%. The resulting design charts provide a practical tool for preliminary shaft assessment without requiring a separate finite-element model for each geometry.*

Keywords: *applied mechanics; stepped shaft; shoulder fillet; stress concentration; combined loading; bending; torsion; design map.*

1. Introduction

Stepped shafts are extensively used for torque transmission, rotating parts support in vehicles, turbines, pumps, machine tools, and in drive systems in industries. The changing of diameters is necessary to locate bearings, gears, pulleys, couplings and retaining elements, but it disrupts the nominal stress field and create local stress concentrations at the shoulder fillet. Experimental, analytical and numerical studies have been conducted to investigate these effects[1][2].

The theoretical stress-concentration factor for circular stepped shafts depends primarily on the diameter ratio D/d, the fillet-radius ratio r/d and the loading mode. Noda[3] designed stress concentration solutions for shoulder fillets under various loading conditions and Tipton[4] revised earlier design-chart values for bending and axial loading. Typically, shafts experience bending and torsional loading simultaneously. Rolovic et al. proved that the maximum bending and torsional stresses can be located at different positions along the fillet, so directly combining separate peak values can give inaccurate or overly conservative equivalent stresses[5]. Later, Tipton[6] presented finite-element based solutions of shoulder-filleted shafts under various loading conditions.

Mayr and Rother suggested equations for circular shafts under individual loading and combined loading including a direct equivalent-stress equation for a wide geometric range[7]. These correlations are helpful in preliminary design as they enable a fast assessment of a large number of geometry and loading combinations without developing a distinct finite-element model for each case. However, finite element analysis will be important for detailed stress assessment and verification, especially because the results are dependent on geometry definition, mesh resolution, and modelling assumptions, as described in[8][9][10].

Several studies have also examined geometric methods to reduce shoulder stress concentration. Compared to the conventional circular fillets, optimized fillet and variable-radius profiles can lead to reduce maximum local stress[11][12][13][14]. If the available fillet radius is restricted, stress relief grooves can be used as an alternative, but can also cause extra geometric and manufacturing requirements [15][16][17]. The importance of the shoulder region also extends to fatigue, where surface condition and machining quality can also be influential on the initiation and life of cracks[18]. Hence, elastic stress-concentration analysis is considered as a preliminary design procedure instead of a fatigue design assessment.

There are several reliable stress-concentration solutions, finite element analyses, and optimized transition profiles available in the literature. There are however many studies that deal with a limited geometric range, a single loading mode, or special fillet shapes. A compact design oriented assessment which simultaneously relates D/d, r/d, and bending–torsion ratio to local von Mises stress and static safety factor is still useful in the preliminary design of a shaft.

This study addresses that need by conducting a parametric assessment of a conventional circular shoulder fillet under combined bending and torsion. For 60 combinations of diameter ratio, fillet-radius ratio and nominal torsion to bending stress ratio, the von Mises stress-concentration factor is evaluated, and is then converted into a local equivalent stress and static safety factor for an illustrative steel shaft. The effects of the governing parameters are quantified, the region of maximum stress reduction is identified, the diminishing benefit of increasing the fillet radius is evaluated, the minimum *r/d* required for a prescribed safety factor is determined, and dimensionless design charts are developed.

The study offers a practical approach to correlate the shaft geometry and combined loading with stress concentration and static safety. By applying an established combined load formulation, it develops design maps and preliminary design recommendations to support shaft design within the method's applicable range.

2. Methodology

2.1 Geometry and dimensionless variables

The investigated shaft geometry and the applied bending moment M_b and torque T are shown in Figure 1.

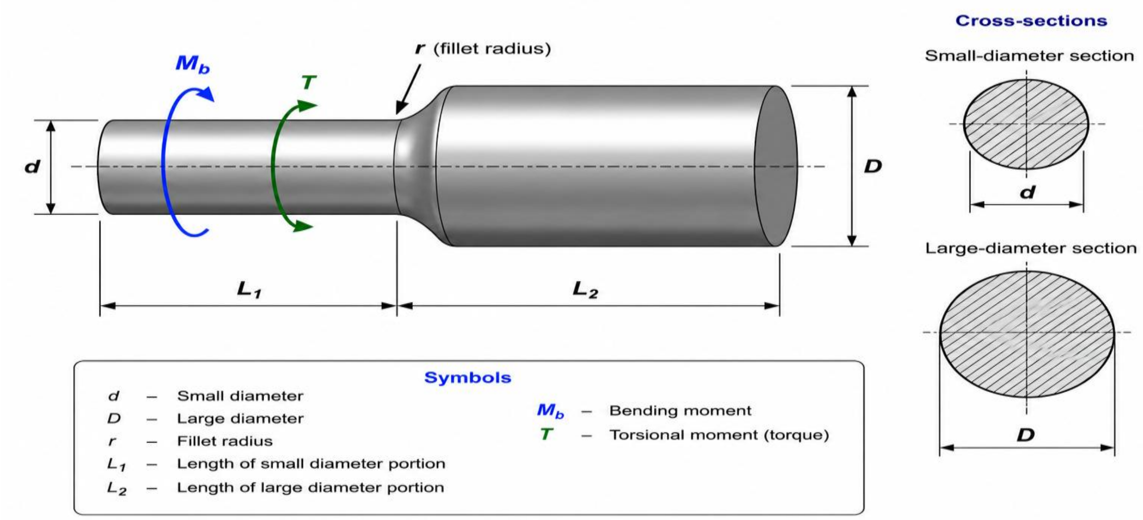

Figure 1. Geometry, dimensional parameters, and loading of the filleted stepped shaft.

The shoulder height is

$$t = \frac{D - d}{2}. \quad (1)$$

The following are the dimensionless geometric variables:

$$q = \frac{D}{d}, \qquad \rho = \frac{r}{d}, \qquad \frac{t}{d} = \frac{q - 1}{2}. \quad (2)$$

where: q, ρ, and t/d are the diameter, fillet-radius, and shoulder-height ratios, respectively.

The loading ratio is defined as

$$\eta = \frac{\tau_t}{\sigma_b}, \quad (3)$$

where: σ_b is the nominal bending stress and τ_t is the nominal torsional shear stress.

The investigated values were

$$\frac{D}{d} = 1.2,\ 1.4,\ 1.6,\ 1.8,$$

$$\frac{r}{d} = 0.02,\ 0.04,\ 0.06,\ 0.08,\ 0.10,$$

and

$$\eta = 0,\ 0.5,\ 1.0.$$

The full factorial combination of four diameter ratios, five fillet ratios, and three loading ratios produced $4 \times 5 \times 3 = 60$ computational cases.

Table 1. Model parameters and investigated ranges

Parameter	**Symbol**	**Value or range**	**Role**
Smaller shaft diameter	d	30 mm	Reference dimension
Diameter ratio	D/d	1.2, 1.4, 1.6, 1.8	Geometric discontinuity
Fillet-radius ratio	r/d	0.02–0.10	Fillet smoothness
Loading ratio	$\eta = \tau_t/\sigma_b$	0, 0.5, 1.0	Bending–torsion combination
Nominal bending stress	σ_b	70 MPa	Reference load level
Yield strength	S_y	355 MPa	Static safety assessment
Required safety factor	n_{req}	1.5	Illustrative design criterion

All 60 geometric combinations were within the specified validity ranges,

$$0.03 \le \frac{r}{t} \le 10, \qquad 0.40 \le \frac{d}{D} \le 0.98.$$

supporting the applicability of the adopted correlation in the investigated domain. The formulation is based on the assumption of linear elasticity and considers the individual and combined loading.

2.2 Nominal stresses and illustrative loads

The nominal stresses were calculated at the smaller diameter section. The corresponding bending stress is

$$\sigma_b = \frac{32M_b}{\pi d^3}, \tag{4}$$

and the nominal torsional shear stress is

$$\tau_t = \frac{16T}{\pi d^3}. \tag{5}$$

The nominal stresses were calculated using the convention adopted in the correlation.

The nominal von Mises stress is

$$\sigma_{\mathrm{vM,nom}} = \sqrt{\sigma_b^2 + 3\tau_t^2}. \tag{6}$$

Using Equation (3),

$$\sigma_{\mathrm{vM,nom}} = \sigma_b\sqrt{1 + 3\eta^2}. \tag{7}$$

A nominal bending stress of

$$\sigma_b = 70 \text{ MPa}$$

was selected to convert the dimensionless factors into illustrative local stresses and safety factors.

For

$$d = 30 \text{ mm},$$

the corresponding bending moment is

$$M_b = \frac{\sigma_b \pi d^3}{32} = 185.55 \text{ N} \cdot \text{m}. \tag{8}$$

From Equations (3) and (5), the torque can be expressed as

$$T = \frac{\eta \sigma_b \pi d^3}{16}. \tag{9}$$

The three loading ratios therefore correspond to:

η	τ_t(MPa)	T(N·m)	Loading interpretation
0	0	0	Pure bending
0.5	35	185.55	Bending-dominated combined loading
1.0	70	371.10	Equal nominal bending and torsional stresses

The load magnitude does not affect the elastic stress-concentration factor; it is used only to calculate the local stress and safety factor.

2.3 Combined-load stress-concentration correlation

The von Mises stress-concentration factor was calculated using the combined-load correlation developed by Mayr and Rother. With the axial stress set to zero, the formulation can be written as

$$K_{\mathrm{vM}} = 1 + \left[A\left(\frac{r}{t}\right) + B\left(\frac{r}{d}\right)\sqrt{1 + 47\frac{r}{d}}\right]^{-1/2}, \tag{10}$$

where

$$A = \frac{1 + 2.9\eta^2}{1 + \eta^2}, \tag{11}$$

and

$$B = \frac{7.8 + 13.8\eta^2}{1 + 0.6\eta^2}. \qquad (12)$$

Equations (10)–(12) have been obtained by setting the nominal axial stress to be zero in the adopted von Mises combined loading formulation, and was fitted to refined linear elastic finite element results for circular shoulder-filleted shafts. This correlation was used in the present study in a parametric analytical–computational evaluation.

To verify the numerical implementation of Equations (10)–(12), A benchmark comparison was made against the pure-bending solution of Tipton. For

$\frac{D}{d} = 1.5,\ \frac{r}{d} = 0.05,\ \eta = 0.$

the adopted correlation gives

$$K_{\mathrm{vM}} = 2.046.$$

For pure bending, K_{vM} is identical to the bending stress-concentration factor. The value quoted by Tipton is about 2.03, which represents a relative difference of

$$\delta = \frac{|2.046 - 2.03|}{2.03} \times 100 = 0.8\%$$

This close agreement will facilitate the proper numerical implementation of the adopted correlation and its application in the following parametric evaluation.

In addition, three representative geometries were selected for the direct finite-element (FE) verification in ANSYS: (D/d, r/d, η) = (1.2,0.02,0.5), (1.6,0.06,1.0), and (1.8,0.10,0). A 3-D models with quadratic SOLID186 elements was employed and a local mesh refinement in the fillet region until the convergence of the maximum equivalent stress was reached. The same nominal bending and torsional loading conditions as in the correlation based analysis were applied. The converged FEA local equivalent stresses were then compared to the corresponding prediction from the correlation; a maximum deviation 2.4% would validate close agreement and make the use of the correlation for preliminary elastic stress screening possible.

2.4 Local stress, severity index, and safety factor

The maximum local equivalent stress was calculated from

$$\sigma_{\mathrm{vM,max}} = K_{\mathrm{vM}}\sigma_{\mathrm{vM,nom}}. \qquad (13)$$

A dimensionless severity index was defined to compare the loading ratios with the same nominal bending-stress reference:

$$\Psi = \frac{\sigma_{\mathrm{vM,max}}}{\sigma_b}. \qquad (14)$$

Substitution of Equations (7) and (13) gives

$$\Psi = K_{\mathrm{vM}}\sqrt{1 + 3\eta^2}. \qquad (15)$$

The static safety factor was calculated as

$$n = \frac{S_y}{\sigma_{\mathrm{vM,max}}}, \qquad (16)$$

where the illustrative yield strength was

$$S_y = 355\ \mathrm{MPa}.$$

A required safety factor of

$$n_{\mathrm{req}} = 1.5$$

was adopted for the design comparison.

The safety factor only considers elastic static screening and excludes fatigue effects, surface condition, residual stress, corrosion, size effects, or manufacturing tolerances.

2.5 Computational procedure

The computational procedure used to evaluate the 60 geometric and loading combinations is summarized in Figure 2.

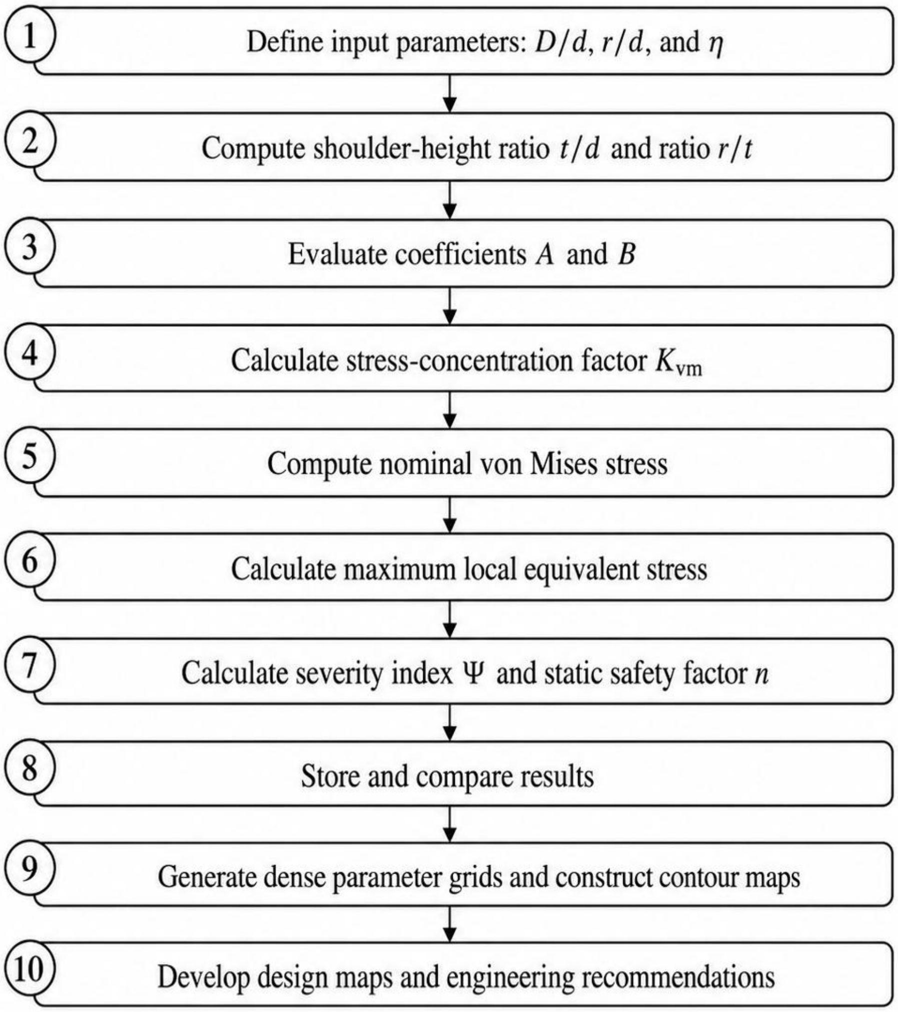

Figure 2. Computational workflow for the parametric analysis and design-map development.

The minimum r/d values listed in Table 3 were computed numerically by applying the bisection method. For the value of $n = n_{req}$, equations (10) and (16) were solved simultaneously with a convergence tolerance of 1×10^{-6}.

3. Results and Discussion

3.1 Effect of fillet-radius ratio

Figures 3 and 4 present the calculated stress concentration factors for pure bending and equal nominal bending and torsional stresses. In all cases, K_{vM} decreased as r/d increased.

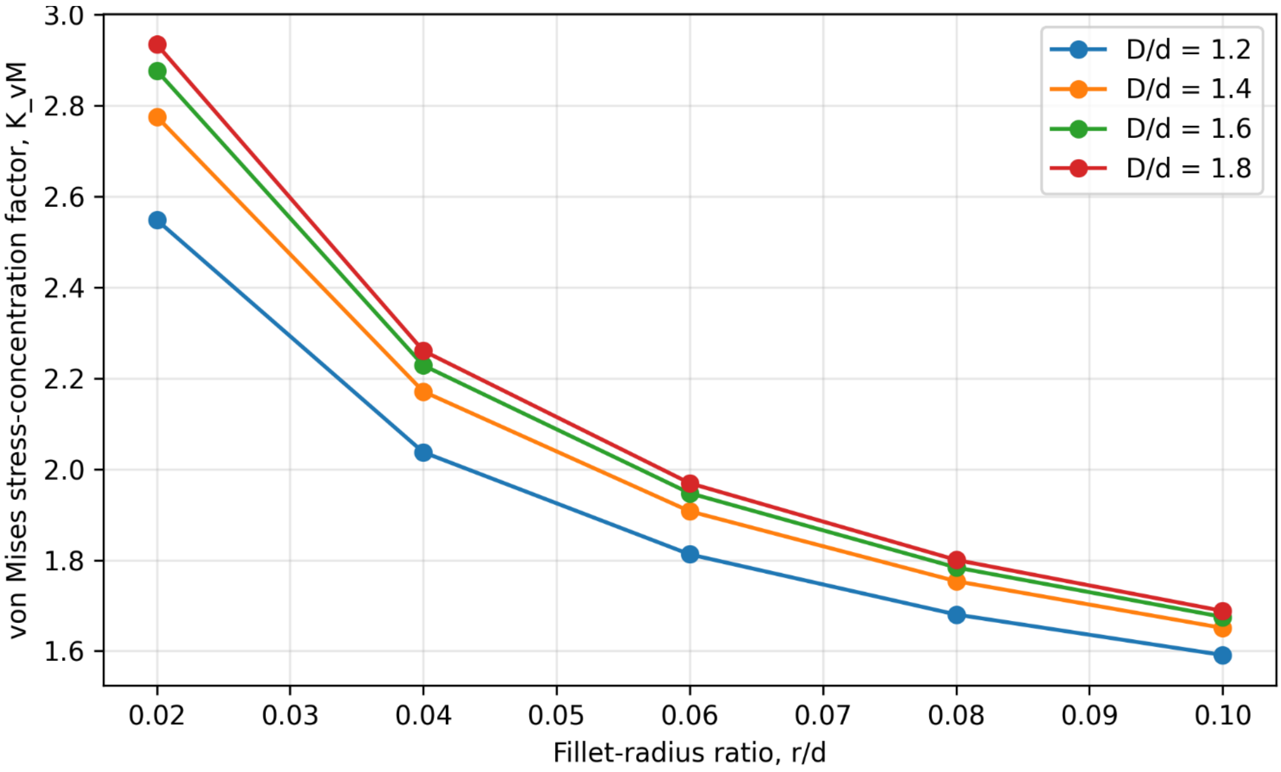

Figure 3. Effect of r/don the von Mises stress-concentration factor under pure bending.

Under pure bending, when r/d was increased from 0.02 to 0.10, K_{vM} was reduced by 37.6% at $D/d = 1.2$ and 42.5% at $D/d = 1.8$. The larger reduction at the higher diameter ratio indicates the more severe initial stress concentration associated with a small fillet.

The lowest pure-bending value was

$$K_{\mathrm{vM}} = 1.591$$

at

$$\frac{D}{d} = 1.2, \qquad r/d = 0.10.$$

The highest pure-bending value was

$$K_{\mathrm{vM}} = 2.934$$

at

$$\frac{D}{d} = 1.8, \qquad r/d = 0.02.$$

The greatest reduction was at small r/d, indicating that increasing a very small fillet is more effective than to further enlarging an already moderate one.

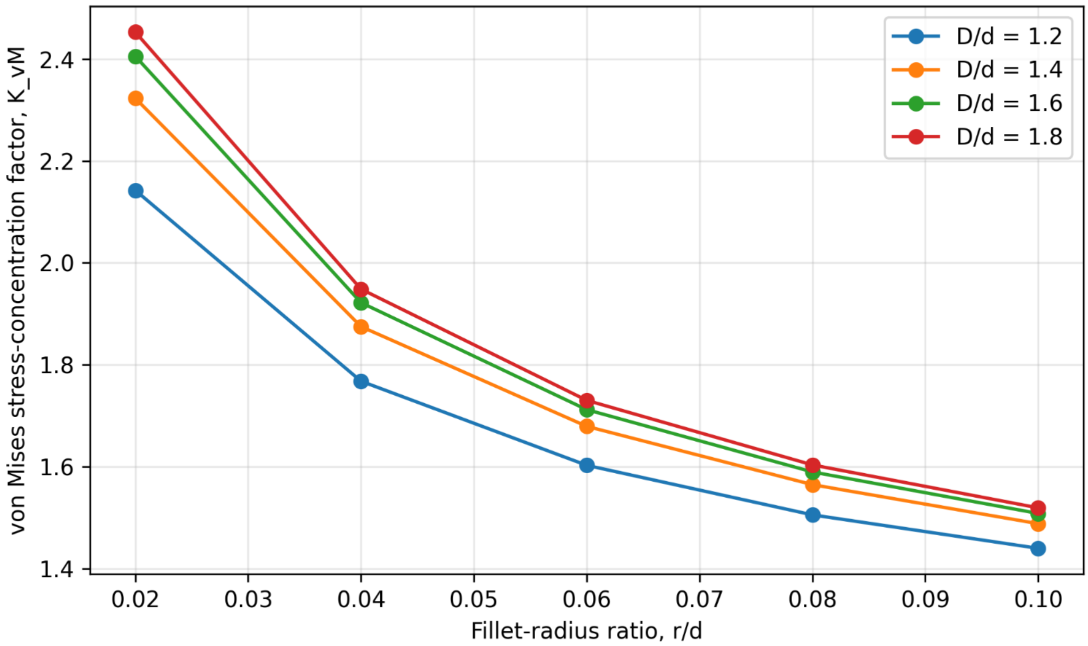

Figure 4. Effect of r/don the von Mises stress-concentration factor at $\eta = 1$.

The same geometric trend was noted at η=1. Increasing r/d from 0.02 to 0.10 reduced K_{vM} by 32.8–38.1%, with values ranging from 1.440 to 2.453. Even though the K_{vM} decreased at the higher torsional contribution, the actual local stress did not, because the nominal equivalent stress increased.

3.2 Effect of diameter ratio

An increase in D/d consistently raised K_{vM} at a fixed r/d,. When D/d increased from 1.2 to 1.8, K_{vM} rose by 15.2% at $r/d = 0.02$ and 6.1% at $r/d = 0.10$ under pure bending. The increases at η=1 were 14.5% and 5.5%, respectively. Therefore, the influence of the diameter ratio is more significant for small fillet radii while a larger fillet partly reduces its adverse influence.

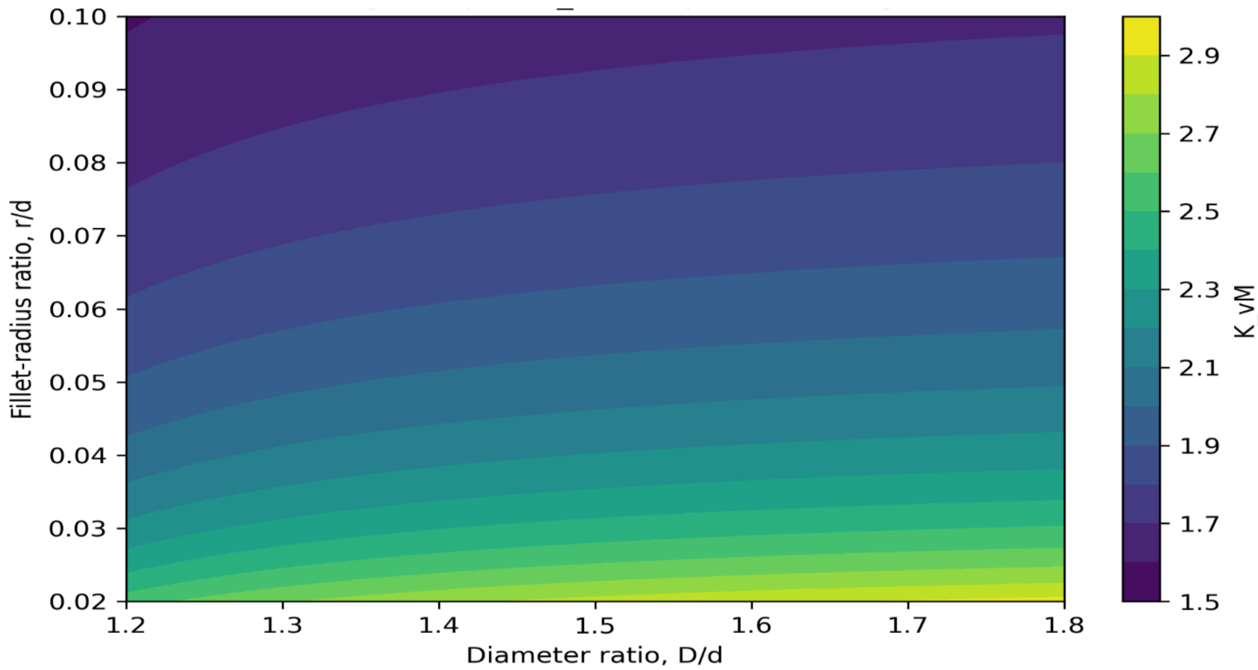

Figure 5. Dimensionless design map of K_{vM} under pure bending.

The contour map shows that K_{vM} is most sensitive to r/d at small fillet radii. In the range of investigated values, increasing r/d reduces stress concentration more effectively than decreasing D/d. Hence, the adverse effect of a larger diameter step is greatest in the case of small fillet radius, and the dominant geometric parameter is r/d.

3.3 Combined loading and maximum local stress

Table 2 summarizes the overall ranges that obtained for the three loading ratios.

Table 2. Summary of calculated results by loading ratio

η	$\sigma_{vM,nom}$**(MPa)**	K_{min}	K_{max}	**Minimum local stress (MPa)**	**Maximum local stress (MPa)**	**Minimum n**	**Maximum n**
0.0	70.0	1.591	2.934	111.4	205.4	1.73	3.19
0.5	92.6	1.519	2.711	140.6	251.1	1.41	2.52
1.0	140.0	1.440	2.453	201.6	343.4	1.03	1.76

The nominal von Mises stress increased from 70 MPa under pure bending to 140 MPa under equal nominal bending and torsional stresses. The maximum local stress increased because of the higher nominal equivalent stress, although K_{vM} decreased.

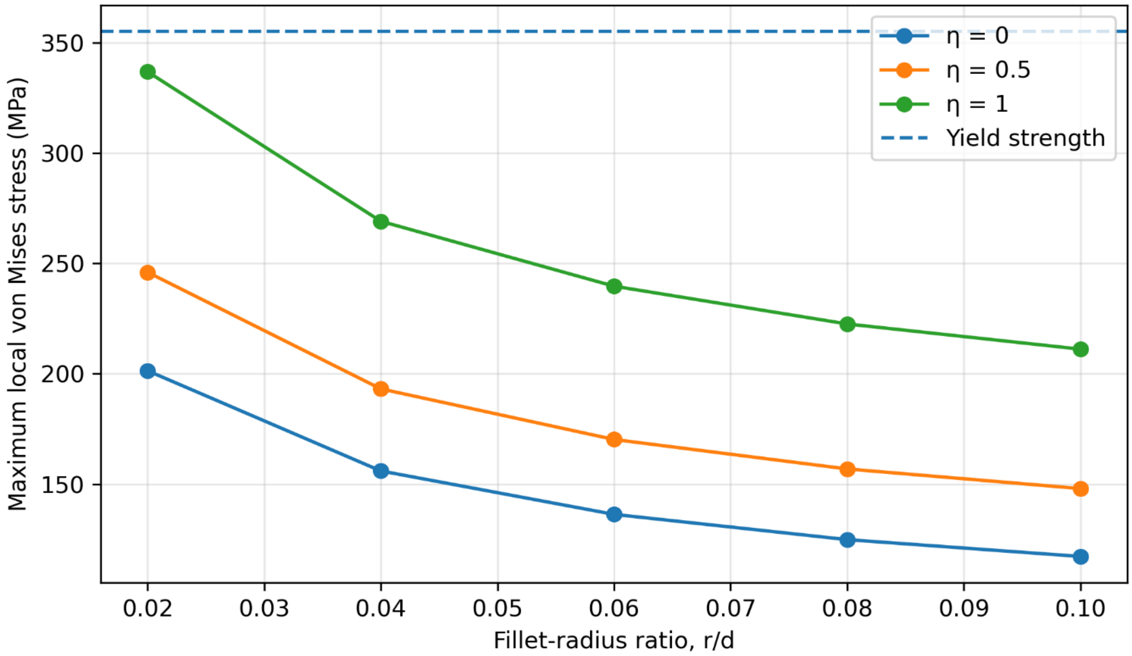

Figure 6. Maximum local equivalent stress at $D/d = 1.6$ for the three loading ratios.

For $D/d = 1.6$, the local equivalent stress increased markedly with η for every radius.

At $r/d = 0.02$, increasing η from 0 to 1:

- reduced K_{vM} by 16.4%;
- increased the maximum local stress by 67.3%.

At $r/d = 0.10$, increasing η from 0 to 1:

- reduced K_{vM} by 10.0%;
- increased the maximum local stress by 80.1%.

The K_{vM} reduction with increasing torsional contribution can be physically associated with the different stress distribution produced by bending and torsion. A pure bending produces maximum normal stress that is highly localized at the critical fillet surface. The torsional shear stress is more evenly distributed around the circumference of the shaft and it's generally less dominated by a single localized bending peak. For the combination of the two components, according to the von Mises criterion, the relative contribution of the bending peak to the normalized equivalent stress is reduced, and thus K_{vM} is decrease.

This reduction is also partly a normalization effect because

$$K_{\mathrm{vM}} = \frac{\sigma_{\mathrm{vM,max}}}{\sigma_{\mathrm{vM,nom}}}$$

And

$$\sigma_{\mathrm{vM,nom}} = \sigma_{\mathrm{b}}\sqrt{1+3\eta^2}$$

This is because K_{vM} is normalized by the nominal equivalent stress, which is raised from 70 MPa at $\eta = 0$ to 140 MPa at $\eta = 1$. The maximum local stress also rises, but less than proportionally to the nominal stress. Thus, the normalized concentration factor gets smaller even if the actual local stress becomes grater. It is therefore A lower K_{vM} in combined loading should not be interpreted as a "safer condition".

The most favorable case in the full matrix was

$$\frac{D}{d} = 1.2, \qquad \frac{r}{d} = 0.10, \qquad \eta = 0,$$

which produced

$$\sigma_{\mathrm{vM,max}} = 111.4\ \mathrm{MPa}$$

and

$$n = 3.19.$$

The most severe case was

$$\frac{D}{d} = 1.8\,, \qquad \frac{r}{d} = 0.02, \qquad \eta = 1,$$

which produced

$$\sigma_{\mathrm{vM,max}} = 343.4\ \mathrm{MPa}$$

and

$$n = 1.03.$$

This case is slightly below the yield strength however, it leaves little static margin and when factors such as fatigue, surface condition, load uncertainty, manufacturing tolerances, or transient load, are taken into consideration, it may not be acceptable.

The present safety factors are based on the yield strength S_{y} and are applicable to elastic static screening. In practice, a rotating shaft is often subjected to cyclic bending and torsion and, may fail by fatigue at stresses below the yield strength. Thus, the corrected endurance limit S_e, fatigue notch factor, mean stress effects, surface finish, size, reliability and loading factors should be included in a complete fatigue assessment. The static safety factors reported, therefore should be treated as preliminary upper-bound indicators rather than fatigue design margins.

3.4 Finite-Element Validation Results

The ANSYS results were compared directly with the corresponding correlation predictions for the three representative cases as defined in Section 2.4. The summary of comparison is presented in Table 3.

Table 3. Comparison between correlation and FEA results

Case	D\d	r\d	η	Correlation stress (MPa)	FEA stress (MPa)	Difference (%)
1	1.2	0.02	0.5	217.6	220.2	1.2
2	1.6	0.06	1.0	239.7	234.6	2.1

3	1.8	0.10	0	118.2	119.9	1.5

The relative difference was evaluated as:

$$\delta = \frac{|\sigma_{FEA} - \sigma_{corr}|}{\sigma_{corr}} \times 100$$

The three cases differed by 1.2%, 2.1%, and 1.5%, respectively, with a maximum deviation of 2.1%. This close agreement supports the consistency of the adopted correlation with the FE response and its applicability to preliminary elastic stress screening.

3.5 Safety-factor map and required fillet radius

All 20 geometries that satisfied $n \geq 1.5$ under pure bending compared with 17 at $\eta = 0.5$ and only 10 at $\eta = 1$.

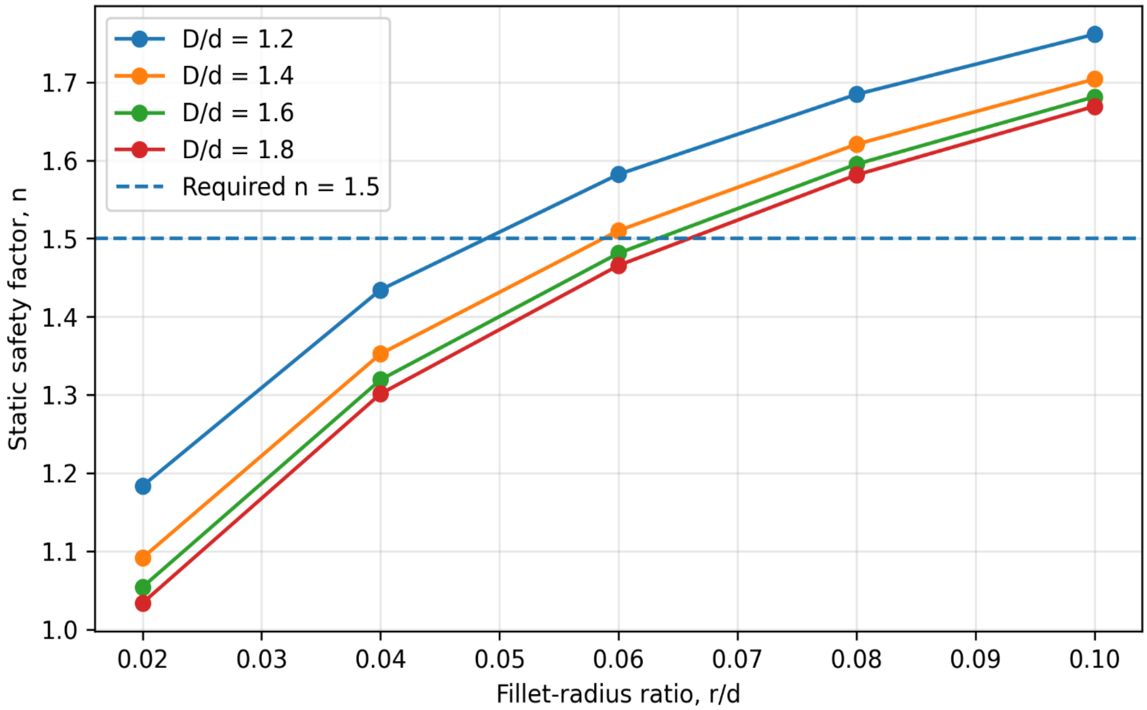

Figure 7. Static safety factor as a function of r/d for $\eta = 1$.

A moderate-to-large fillet is needed for equal stress case over the range of D/d investigated. The intersections with $n = 1.5$ provide the approximate minimum acceptable r/d and the continuously solved values are listed in Table 4.

Table 4. Minimum r/d required to obtain $n = 1.5$

D/d	$\eta = 0$	$\eta = 0.5$	$\eta = 1.0$
1.2	0.0091	0.0155	0.0479
1.4	0.0120	0.0201	0.0585
1.6	0.0133	0.0222	0.0629
1.8	0.0141	0.0234	0.0653

Values lower than 0.02 (for $\eta = 0$ and $\eta = 0.5$) are out of the parametric range investigated in this study (0.02–0.10) but still within the range of validity of the adopted correlation ($0.03 \leq r/t \leq 10$). The extrapolated values should be used cautiously in the preliminary design and confirmed with detailed FE analysis in the final design.

Under equal nominal bending and torsional stresses, the required r/d increased from 0.0479 at $D/d = 1.2$ to 0.0653 at $D/d = 1.8$.

For the discrete design levels used in the main matrix, the results are roughly corresponding to:

$$r/d \geq 0.06$$

for D/d up to approximately 1.4, and

$$r/d \geq 0.08$$

for $D/d = 1.6$–1.8.

These values are specific to

$$\sigma_b = 70 \text{ MPa}, \qquad S_y = 355 \text{ MPa}, \qquad n_{\text{req}} = 1.5.$$

The same procedure can be applied for other materials, load levels, or required safety factors.

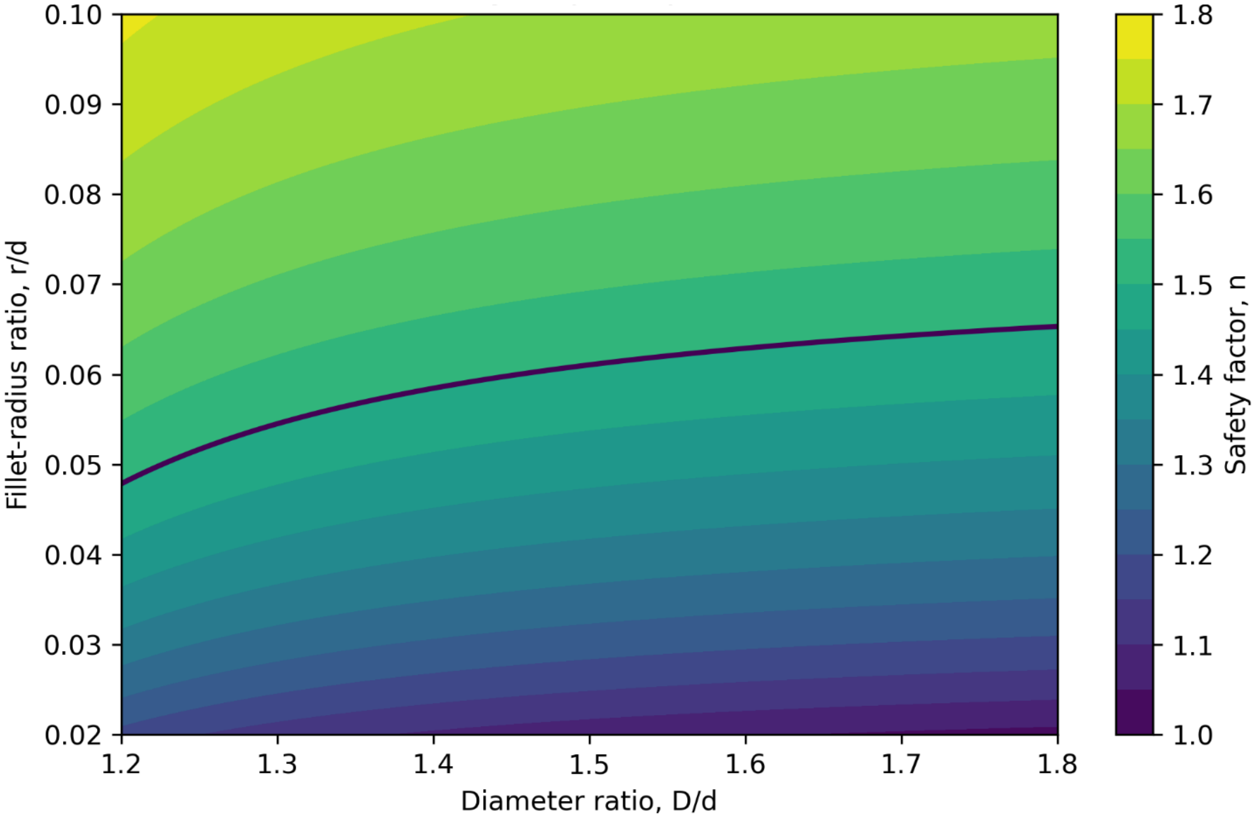

Figure 8. Safety-factor map for $\eta = 1$; the contour line indicates $n = 1.5$.

The contour line separates the acceptable and unacceptable regions for the illustrative static criterion. In contrast to single recommended radius, the map shows the trade-off between D/d and r/d. A larger diameter ratio can be compensated by increasing the fillet ratio, while a limitation on the available fillet radius may necessitate a smaller diameter step.

3.6 Diminishing benefit of increasing the fillet radius

The average value of K_{vM}, calculated across all diameter and loading ratios, decreased from 2.561 at $r/d = 0.02$to 1.572 at $r/d = 0.10$.

However, the incremental benefit diminished with each successive increase in r/d:

Increase in r/d	Reduction in mean K_{vM}
0.02 to 0.04	20.8%
0.04 to 0.06	11.4%
0.06 to 0.08	7.5%
0.08 to 0.10	5.4%

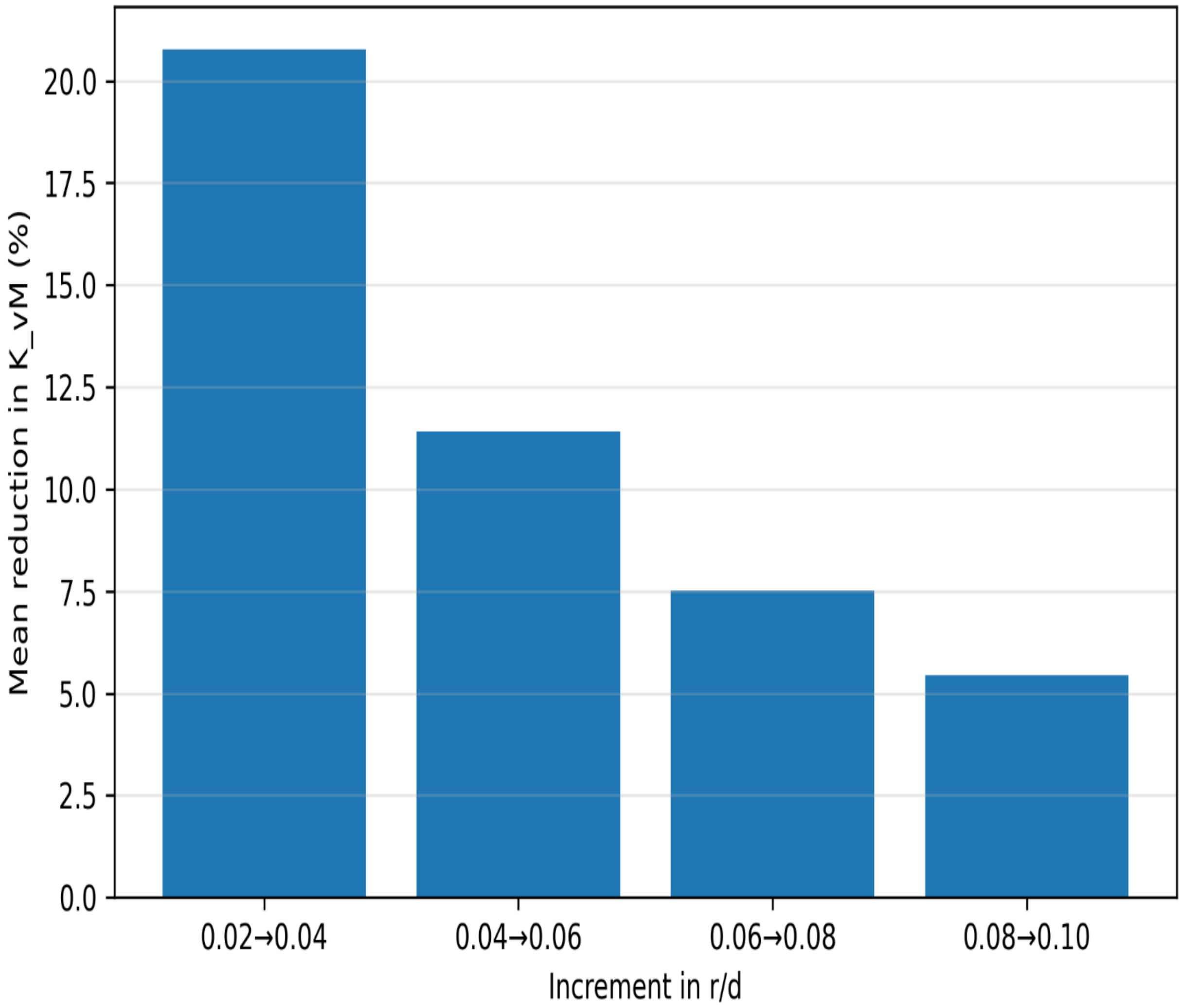

Figure 9. Mean reduction in K_{vM} obtained from successive increases in r/d.

The results show that diminishing returns with increasing r/d. The largest improvement is seen as the fillet ratio is increased from a very small value to $r/d = 0.04$, but additional increases yield smaller benefits. For practical designs, $r/d \approx 0.06$–0.08 can therefore be considered a reasonable compromise, particularly when the shoulder must accommodate bearings, retaining rings, spacers, or other mounted components.

3.7 Relation to previous studies

The comparison between the present results and previous studies is summarized in Table 5.

Table 5. Comparison with previous studies

Aspect	Previous studies	Present results
Fillet radius	Larger fillets reduce stress concentration.	Increasing r/d from 0.02 to 0.10 reduced K_{vM} by 32.8–42.5%.
Diameter ratio	Larger diameter steps increase stress concentration.	Increasing D/d from 1.2 to 1.8 raised K_{vM} by 5.5–15.2%.
Fillet profile	Optimized profiles reduced stress by up to 15%.	A conventional circular fillet achieved reductions of up to 42.5% by increasing r/d.
Combined	Independent peak factors	At the critical

loading	should not be directly combined because their maxima may occur at different fillet positions.	geometry, K_{vM} decreased by 16.4%, while local stress increased by 67.3%.
Contribution	Previous studies focused mainly on stress prediction or shape optimization.	The present method links geometry, loading, local stress, and static safety factor.

The novelty of this work is that Ref. gave the generalized correlation, but in the present work, it is converted into explicit design maps and discrete tables directly correlating the minimum required fillet-radius ratio r/d to a prescribed static safety facto. This design-oriented interpretation is not covered in the original correlation study.

To demonstrate the practical use of the design maps, let consider a steel shaft with

d=40 mm, d\D=1.6,

subjected to

$\sigma_b = 80$ MPa, $\tau_t = 40$ MPa,

giving

$\eta = \tau_t \backslash \sigma_b = 0.5$.

For

$S_y = 400$ MPa and $n_{req} = 1.5$,

Table 4 provides the required fillet-radius ratio for

r\d = 0.0222.

Then the radius of the corresponding fillet is

r = 0.0222(40) = 0.888 mm.

If the available fillet radius is limited to 0.60 mm, then

r\d = 0.60 \ 40 = 0.015,

which is less than the required value. If the diameter ratio is reduced to D/d=1.4, the minimum required ratio is reduced to r/d = 0.0201, corresponding to

r = 0.0201(40) = 0.804 mm.

This value is still greater than the available radius of 0.60 mm, and the designer should make further improvements on them, such as reducing D/d, increasing the fillet radiuses, or increasing the strength of the material or reducing the loading. This step-by-step procedure demonstrates how the proposed tables can serve as a quick preliminary-design tool, without the need to perform iterative finite element modelling for each candidate geometry.

4. Conclusions

A dimensionless parametric assessment of a circular filleted stepped shaft subjected to combined bending and torsion was performed with 60 combinations of D/d, r/d and η. A finite element - based correlation was used to calculate K_{vM}, local equivalent stress and static safety-factor maps. The main conclusions are: The most significant parameter was the fillet-radius ratio. Increasing r/d from 0.02 to 0.10 reduced K_{vM} by 32.8–42.5%. The increase of D/d from 1.2 to 1.8 lead to increase of K_{vM} by 5.5–15.2% with the strongest effect at small fillet radii. The maximum benefits were obtained when r/d increased from 0.02 to 0.04, which lowered the mean stress-concentration factor by 20.8%. Further increases gave smaller improvements. A lower K_{vM} did not always mean a lower local stress, since the nominal equivalent stress increased with torsional loading. The most severe case (D/d=1.8, r/d=0.02, η=1) reached 343.4 MPa with a static safety factor of 1.03. For $\eta = 1$, achieving $n = 1.5$ required r/d to increase from 0.0479 to 0.0653 as D/d increased from 1.2 to 1.8. The numerical verification confirmed with the adopted methodology. The benchmark comparison with Ref. demonstrated a difference of approximately 0.8%, and the three representative FEA cases demonstrated a difference of 1.2-2.1% from the correlations. The procedure proposed provides a simple and reproducible basis for preliminary fillet-radius selection using shaft geometry, loading, material strength, and safety factor. It serves as an elastic static screening and should be followed by detailed FE and fatigue verification of the final design.

References

[1] I. M. Allison, "The elastic stress concentration factors in shouldered shafts—Part I: Shafts subjected to torsion," *Aeronautical Quarterly*, vol. 12, no. 2, pp. 189–199, 1961, doi: 10.1017/S0001925900002043.

[2] A. Ajovalasit, V. Nigrelli, G. Pitarresi, and G. Virzì Mariotti, "On the history of torsional stress concentrations in shafts: From electrical analogies to numerical methods," *Journal of Strain Analysis for Engineering Design*, vol. 49, no. 6, pp. 452–466, 2014, doi: 10.1177/0309324714530123.

[3] N.-A. Noda, Y. Takase, and K. Monda, "Stress concentration factors for shoulder fillets in round and flat bars under various loads," *International Journal of Fatigue*, vol. 19, no. 1, pp. 75–84, 1997, doi: 10.1016/S0142-1123(97)82050-6.

[4] S. M. Tipton, J. R. Sorem, and R. D. Rolovic, "Updated stress concentration factors for filleted shafts in bending and tension," *Journal of Mechanical Design*, vol. 118, no. 3, pp. 321–327, 1996, doi: 10.1115/1.2826887.

[5] R. D. Rolovic, S. M. Tipton, and J. R. Sorem, "Multiaxial stress concentration in filleted shafts," *Journal of Mechanical Design*, vol. 123, no. 2, pp. 300–303, 2001, doi: 10.1115/1.1352023.

[6] S. M. Tipton, C. Schmidt, and J. R. Sorem, "Stress concentration factor solutions for shoulder filleted shafts in bending, including the influence of tapering," *SAE International Journal of Materials and Manufacturing*, vol. 4, no. 1, pp. 638–650, 2011, doi: 10.4271/2011-01-0486.

[7] C. M. Mayr and K. Rother, "Improved stress concentration factors for circular shafts for uniaxial and combined loading," *Materials Testing*, vol. 61, no. 3, pp. 193–203, 2019, doi: 10.3139/120.111305.

[8] A. J. Muminovic, I. Saric, and N. Repcic, "Numerical analysis of stress concentration factors," *Procedia Engineering*, vol. 100, pp. 707–713, 2015, doi: 10.1016/j.proeng.2015.01.423.

[9] A. P. Singh, S. Vidya, P. Suresh, A. Kumar, and K. S. Srikanth, "Comparative stress analysis of round shaft with shoulder fillet using finite element and analytical method," *Materials Today: Proceedings*, vol. 56, part 1, pp. 497–501, 2022, doi: 10.1016/j.matpr.2022.02.168.

[10] P. Sivák, I. Delyová, and J. Bocko, "Comparison of stress concentration factors obtained by different methods," *Applied Sciences*, vol. 13, no. 24, Art. no. 13328, 2023, doi: 10.3390/app132413328.

[11] S. S. Bhavikatti and C. V. Ramakrishnan, "Optimum shape design of shoulder fillets in tension bars and T-heads," *International Journal of Mechanical Sciences*, vol. 21, no. 1, pp. 29–39, 1979, doi: 10.1016/0020-7403(79)90074-2.

[12] F. O. Sonmez, "Optimal shape design of shoulder fillets for flat and round bars under various loadings," *Proceedings of the Institution of Mechanical Engineers, Part C: Journal of Mechanical Engineering Science*, vol. 223, no. 8, pp. 1741–1754, 2009, doi: 10.1243/09544062JMES1457.

[13] N. L. Pedersen, "Aspects of stress in optimal shaft shoulder fillet," *Journal of Strain Analysis for Engineering Design*, vol. 53, no. 5, pp. 285–294, 2018, doi: 10.1177/0309324718763514.

[14] J. T. P. de Castro, D. de A. Simões, I. F. M. de Menezes, M. A. Meggiolaro, and L. F. Martha, "A note on notch shape optimization to minimize stress concentration effects," *Theoretical and Applied Fracture Mechanics*, vol. 84, pp. 72–85, 2016, doi: 10.1016/j.tafmec.2016.03.005.

[15] J.-M. Shin, D.-S. Han, K.-H. Lee, and S.-H. Han, “Using stress relief grooves to reduce stress concentration on axle drive shaft,” *Journal of Mechanical Science and Technology*, vol. 28, no. 6, pp. 2121–2127, 2014, doi: 10.1007/s12206-014-0409-7.

[16] J. M. González-Mendoza, S. Alcántara-Montes, J. de J. Silva-Lomelí, C. de la Cruz-Alejo, and A. Ocampo-Ramírez, “Size optimization of shoulder filleted shafts with relief grooves for improving their fatigue life,” *Ingeniería e Investigación*, vol. 37, no. 3, pp. 85–91, 2017, doi: 10.15446/ing.investig.v37n3.57957.

[17] M. Kubota, S. Kataoka, and Y. Kondo, “Effect of stress relief groove on fretting fatigue strength and index for the selection of optimal groove shape,” *International Journal of Fatigue*, vol. 31, no. 3, pp. 439–446, 2009, doi: 10.1016/j.ijfatigue.2008.07.007.

[18] X. Zhu, Z. Dong, Y. Zhang, and Z. Cheng, “Fatigue life prediction of machined specimens with the consideration of surface roughness,” *Materials*, vol. 14, no. 18, Art. no. 5420, 2021, doi: 10.3390/ma14185420.